CELLULOSE (1995) 2, 111–127

Ultrastructural aspects of the acetylation of cellulose

JEAN-FRANÇOIS SASSI AND HENRI CHANZY*
Centre de Recherches sur les Macromolécules Végétales, (CERMAV-CNRS), B.P. 53, 38041 Grenoble Cédex 9 (affiliated with the Joseph Fourier University of Grenoble), France

An ultrastructural study of the acetylation of cellulose was achieved by subjecting well characterized cellulose samples from *Valonia* cell wall and tunicin tests to homogeneous and heterogeneous acetylation. The study involved transmission electron microscopy observations on negatively stained microcrystals as well as diffraction contrast images of the cross sections of wall fragments at various stages of the reaction. These observations showed that the acetylation of crystalline cellulose proceeds by a reduction of the diameters of the crystals while their lengths are reduced to a lower extent. These results were corroborated by electron and X-ray diffraction experiments that showed that during the reaction there was a rapid decrease in the intensities of the equatorial diffraction spots of cellulose, whereas those located on the meridian or close to the meridian stayed constant. A model of acetylation of the cellulose crystal is presented. It is based on a non swelling reaction mechanism that affects only the cellulose chains located at the crystal surface. In the case of homogeneous acetylation, the partially acetylated molecules are sucked into the acetylating medium as soon as they are sufficiently soluble. In heterogeneous conditions the cellulose acetate remains insoluble and surrounds the crystalline core of unreacted cellulose.

KEYWORDS: acetylation; cellulose acetate; *Valonia*; tunicin; cellulose microcrystals

INTRODUCTION

In the current process of acetylation of cellulose, fibres of native cellulose are gradually converted into cellulose triacetate (CTA) upon the addition of a dry mixture of acetic anhydride and acetic acid in the presence of a small amount of catalyst such as sulfuric or perchloric acid (Tanghe *et al.*, 1963; Serad, 1985). Depending on the presence or not of a non swelling diluent, two acetylation mechanisms can be distinguished. In the so-called 'fibrous process', diluents such as toluene, benzene or amyl acetate are added to the reaction medium. Under such conditions, CTA remains insoluble and there is a direct conversion of cellulose into solid CTA without change in the gross morphology of the fibres (Buras *et al.*, 1957; Sprague *et al.*, 1958). In the more common solution or 'homogeneous' process where there is no diluent (Malm *et al.*, 1946; Tanghe *et al.*,

*To whom correspondence should be addressed.
0969-0239 © 1995 Blackie Academic & Professional

1963), CTA is solubilized in the reaction medium as it is produced. In this case, the cellulose fibres undergo substantial morphological changes before their total acetylation and concomitant dissolution.

The acetylation of cellulose is a typical heterogeneous reaction. It depends on the one hand on the accessibility of the cellulose elements within the starting cellulosic fibres and on the other on the susceptibility of the individual cellulose crystallites toward acetylation. The rate and perfection of acetylation is therefore greatly influenced by the macro and micro morphology of the initial cellulose fibres. This is why a number of structural studies have been undertaken in the past to follow the progress of acetylation within given cellulose fibres. These studies, achieved essentially by X-ray analysis (Hess and Trogus, 1931; Conrad and Creely, 1962; Glegg *et al.*, 1968) and optical microscopy (Hess and Schultze, 1927; Kanamaru, 1934; Staudinger *et al.*, 1953) have led to the description of an acetylation scheme where the reaction seems to start within the amorphous regions of cellulose. In a second step, the acetylation of the crystallites themselves takes place. This step is described as an erosion mechanism with the acetylation beginning at the exterior of the crystallites and progressing towards their centre (Sisson, 1938; Glegg *et al.*, 1968). This erosion mechanism explains in particular why a crystalline core of unreacted cellulose may coexist with peracetylated cellulose chains, even when the acetylation process is almost complete. Up to now, the erosion mechanism is still a working hypothesis that has not been substantiated by any ultrastructural observation. In addition, the relative role of the accessibility and reactivity parameters in the acetylation process is not known in detail.

In the last decade, our knowledge of the crystalline ultrastructure of cellulose has progressed substantially thanks to new developments in high resolution electron microscopy and electron diffraction analysis. These techniques applied to large cellulose microfibrils such as those found in the cell walls of *Valonia* and other seaweeds were able to reveal the perfection of the crystalline lattice of cellulose occurring in these specimens. In such samples, the cellulose microfibril appears to be the basic structural element. Each microfibril consists of a monocrystalline continuous cellulose whisker with few or almost no defects (Chanzy, 1990): this is revealed either by observing directly the lattice of cellulose within the microfibrils (Sugiyama *et al.*, 1985a; Sugiyama *et al.*, 1985b; Revol, 1985; Kuga and Brown, 1987a) or recording on each of them sharp spot electron diffraction patterns when 'micro' or 'nano' electron diffraction conditions are selected (Sugiyama *et al.* 1991; Revol and Goring, 1983). These techniques have also been applied with success to cellulose samples of lower perfection such as ramie and bacterial cellulose (Kuga and Brown, 1987a, 1987b). The results seem to indicate that the structural model of *Valonia* cellulose can be transposed to cellulose materials of lower perfection, the difference being in the lateral dimension of the microfibrils and in the amount and location of the amorphous phase.

The present work, which takes advantage of the recent progress in the structural knowledge of cellulose, was undertaken to try to model the course of acetylation of cellulose at the ultrastructural level. For this purpose, batches of well characterized cellulose crystals, either isolated or still within their native environment, were acetylated under either homogeneous or heterogeneous conditions. The course of the reaction, which was monitored by infrared spectroscopy, was followed by diffraction contrast transmission electron microscopy together with X-ray and electron diffraction analysis.

MATERIALS AND METHODS

Cellulose samples

Animal cellulose

Halocynthia roretzi specimens (a kind gift from Professor T. Okano, Tokyo) were used for the preparation of animal cellulose microcrystals. Whole tunics were washed under tap water and separated from the inner body. They were then cut into pieces and soaked overnight at room temperature in a 5% (w/w) aqueous KOH solution. After rinsing with distilled water, they were bleached for 6 h at 80 °C with a 50:50 (v/v) mixture of a 1.7% (w/w) aqueous sodium chlorite solution and an acetate buffer (pH 4.5). The bleaching solution was changed every two hours. The KOH/bleaching treatment was repeated three times, until the tunic fragments became completely white. They were then thoroughly washed with distilled water. After adding a few drops of chloroform as a protectant, they were stored in distilled water until further use.

Microcosmus fulcatus specimens were used for ultrathin sectioning experiments. They were harvested in the Mediterranean sea and anesthetized with chloroform to prevent the contraction of the tunic under pain or stress. The tunics were then slit open and separated from the inner animal body under tap water. Lamellae from the fundamental layer of the tunic were cut parallel to the tunic surface and rinsed several times with distilled water. When checked with infrared spectroscopy, the lamellae contained only cellulose. They were stored in distilled water, after adding a few drops of chloroform as a protectant. These lamellae were used without further purification in acetylation experiments.

Valonia cellulose

Valonia ventricosa vesicles were harvested on the Atlantic seabed in the Lower Keys (Florida). The fresh cells were slit opened and emptied and their walls allowed to dry by pressing between two sheets of tissue paper. The dried cell walls were boiled three times for 3 h in distilled water, and thereafter three times for 2 h in aqueous 0.1 N NaOH under nitrogen. After rinsing with distilled water, they were left overnight at room temperature in an aqueous 0.05 N HCl solution. They were then thoroughly rinsed with distilled water and cut into pieces of a few square millimeters each. In each piece, the two main microfibrillar orientations were determined by X-ray diffractometry. These samples were stored in ethanol.

Cellulose microcrystals

Cellulose microcrystals were prepared by hydrolysis with sulfuric acid following the method of Revol *et al.* (1992). Cellulose fragments were first disintegrated in distilled water with a Waring blender. Sulfuric acid was then added slowly to the suspension of fragments to reach a final acid concentration of 65% (w/w). For *Valonia* as well as *Halocynthia* cellulose, the initial concentration of cellulose was 1% (w/w). The mixture was then heated either to 70 °C (*Valonia* cellulose) or to 80 °C (tunicate cellulose) for 30 minutes under strong stirring. A dispersion of cellulose microcrystals resulted. This dispersion was washed with distilled water by successive centrifugations until a turbid

supernatant was observed. The suspension was then filtered through a fritted-glass filter of porosity 1 (with pore size 90–150 μm) in order to remove the remaining coarse particles. The microcrystal suspension was further purified through dialysis against distilled water until neutrality. The dispersion of cellulose microcrystals was completed by a five minute ultrasonic treatment (B12 Branson sonifier). The aqueous suspensions were kept in the refrigerator after adding a few drops of chloroform as protectant.

Acetylation procedures

Cellulose samples (microcrystals or whole fragments) were washed with glacial acetic acid by successive centrifugations and resuspensions. The quantity of water remaining in the suspensions after washing with acetic acid was determined by Karl-Fischer coulometric titration using a Metrohm KF 684 apparatus. The remaining water (about 2% w/v) was eliminated prior to acetylation by adding an equimolar amount of acetic anhydride.

Homogeneous acetylation

Cellulose (100 parts) dispersed in glacial acetic acid (26000 parts) was heated to 60 °C under strong stirring. A catalytic amount of 95% sulfuric acid was then added (20 parts contained in 434 p of a 4.6% (w/w) mixture with 100% acetic acid). After 5 min, 2500 parts of 98% acetic anhydride were added. Aliquots were taken at selected reaction times and poured into aqueous acetic acid (80%, w/w) in order to terminate the acetylation reaction.

Fibrous acetylation

Cellulose (100 parts) dispersed in 100% acetic acid (26000 parts) was poured under strong stirring and at room temperature into a mixture of 100% acetic acid (58000 parts), 99% toluene (86000 parts) and 70% perchloric acid (4175 parts). After 1 min, 54000 parts of 98% acetic anhydride were added. Aliquots were taken at selected reaction times. They were washed by centrifugation, twice with ethanol and three times with distilled water.

Ultrathin sectioning

Microcosmus tunic and *Valonia* cell wall fragments were removed from the reaction medium at different reaction times. They were washed in 80% (w/w) acetic acid and then with distilled water before being embedded in an aqueous melamine resin (Nanoplast FB 101, Bachhuber and Frösch, 1983). Ultrathin sections about 50 nm thick were cut with an LKB Ultrotome IV ultramicrotome equipped with a low angle diamond knife (Diatome Ultra 35°). For *Valonia* cellulose, the sectioning was achieved perpendicular to one of the two major microfibrils orientations. On the other hand, for *Microcosmus* cellulose, the cutting direction was at random, due to the chiral nematic organization of the microfibrils in the tunic. Ultrathin sections were collected on carbon coated copper grids.

Transmission electron microscopy

All observations and diffraction experiments were achieved with a Philips EM 400 T electron microscope.

For the specimens of microcrystalline cellulose, a drop of each sample was deposited and allowed to dry on a carbon coated copper grid, previously irradiated for 8 h with an UV lamp. For imaging purposes the samples were negatively stained with a 2% uranyl acetate aqueous solution and observed at an accelerating voltage of 80 kV. The images were recorded on Kodak electron microscope films (KEM 4489) at a magnification of 22 000 ×. For electron diffraction, the microscope was operated at an accelerating voltage of 120 kV under low dose conditions. Electron diffraction diagrams were recorded on Mitsubishi electron microscope films (MEM) at a camera length of 150 mm.

The imaging of the ultrathin sections in diffraction contrast mode was achieved at liquid nitrogen temperature and under low dose conditions at 120 kV. Bright field images were obtained using an objective aperture of 20 μm that cuts out the strong diffraction spots of cellulose. The samples were positioned on a Gatan cryo specimen holder which was cooled with liquid nitrogen after inserting the specimen into the microscope column. Ice contamination was prevented with the use of a Gatan anticontaminator. The images were recorded at a magnification of 17 000 × on Agfa Scientia EM plates, developed in Agfa G150 (1 + 3) developer.

X-ray diffraction

All X-ray experiments were achieved with a Philips PW 1720 X-ray generator operated with Cu Kα radiation and equipped with a Warhus vacuum camera. X-ray diffraction diagrams were recorded on Kodak Direct Exposure films. Their radial intensity distribution was traced using an MK III C Joyce-Loebl microdensitometer.

The specimens of *Microcosmus* tunic or *Valonia* cell wall, removed from the reaction medium at different acetylation times, were washed, dried and mounted flat onto 0.02 inch-diameter collimators.

Partially acetylated microcrystalline cellulose specimens were first freeze-dried and then submitted to an hydrolytic treatment (Glegg *et al.*, 1968) that removed most of the cellulose acetate from the residual unreacted cellulose. After thorough washing and drying, the samples were inserted into thin wall glass capillaries which were mounted in the X-ray camera.

All the samples resulting from the heterogeneous acetylation experiments were first annealed at 200 °C for ten minutes under nitrogen prior to X-ray experiments.

Infrared spectroscopy

A Fourier transform infrared spectrophotometer (Perkin Elmer 1720 X) equipped with a microfocus accessory was used throughout this study. Thin films of the specimens were mounted on micro disk sample holders perforated by a 500-μm-diameter hole. The spectra were recorded in the transmission mode in the range 4000–500 cm^{-1}. They resulted from the accumulation of 16 scans at a resolution of 2 cm^{-1}. For comparison,

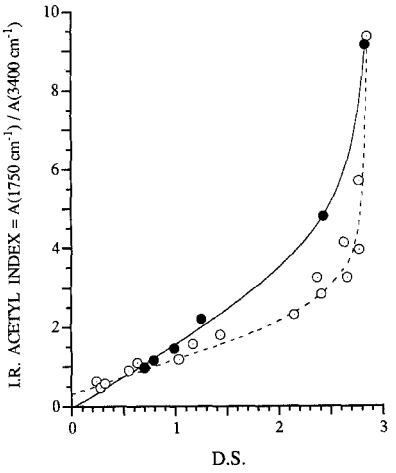

FIGURE 1. Plot of infrared acetyl index as a function of the degree of substitution. (●) our data; (○) data from Hurtubise (1962).

they were adjusted to the same baseline and the band height at 1060 cm^{-1}, corresponding to the C–O stretchings of the glucopyranose ring, was set to 100%.

The acetyl content of the specimens removed from the acetylation medium at different reaction times was evaluated by infrared spectroscopy using the infrared acetyl index method developed by Hurtubise (1962). Cellulose acetates having DS of 0.70, 0.79, 0.99, 1.25 (gifts from J. Hyatt from Eastman Chemical Co, Kingsport, U.S.A), 2.44 (a gift of Rhône-Poulenc Tubize Plastics, Tubize, Belgium) and 2.89 (purchased from Janssen Chimica) were used as standards to draw the master curve shown in Fig. 1, where our experimental data are plotted, together with the calibration curve reproduced from Hurtubise (1962). This master curve was used to calibrate the samples in the course of an acetylation run. This is exemplified in Fig. 2, which corresponds to the homogeneous acetylation of a batch of cellulose microcrystals from tunicin.

RESULTS

When the cellulose microfibrils from *Valonia* cell wall as well as those from *Halocynthia* tunics are acetylated, they first undergo a substantial reduction in diameter. In a subsequent step, they lose their crystalline cohesion. The initial reduction in microfibril diameter is illustrated in Figs 3 and 4, which correspond to microfibrils cross sectioned perpendicular to their long dimensions. As these microfibrils are monocrystalline, they are seen as black objects, due to the bright field diffraction contrast mode that was used to record the pictures. Figures 3a and b correspond to *Valonia*. Initially, in Fig. 3a, the crystalline microfibrils in cross section have their familiar squarish shape (Revol, 1982, Sugiyama, 1985b, Chanzy *et al.*, 1986). They are organized in rows of about three layers thick, each microfibril having a lateral dimension of the order of 10 to 20 nm. Upon acetylation (Fig. 3b), the microfibrils are no longer packed into rows. Their squarish section is lost and their lateral size is drastically reduced. Nevertheless, they are still observed with a strong black contrast, indicating that they still correspond to

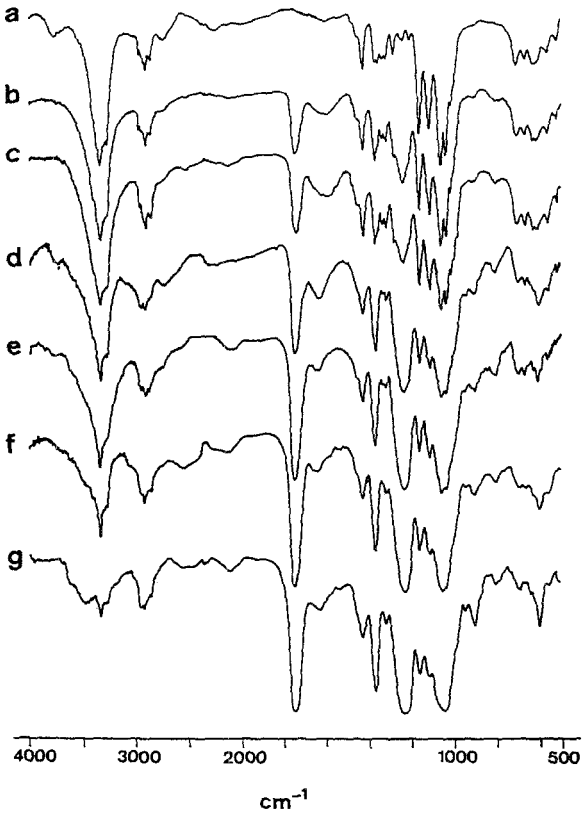

FIGURE 2. A typical series of infrared spectra recorded during the homogeneous acetylation of cellulose microcrystals from tunicate. (a) initial sample; (b) DS 0.14; (c) DS 0.17; (d) DS 0.37; (e) DS 0.86; (f) DS 2.41; (g) DS 2.81.

cellulose monocrystals of perfect or nearly perfect cohesion. Quite interestingly, the sections of the unreacted cellulose cores of the microfibrils are now polygonal, as if entire fragments had been lost during acetylation.

Figures 4a and 4b correspond to cross sections of microfibrils of tunicate cellulose before and after acetylation. In Fig. 4a can be recognized the classical parallelogram-shaped sections of these mono-crystalline elements (Van Daele *et al.*, 1992). Upon acetylation, there is also a reduction in the diameter of the crystalline core of the microfibrils (Figure 4b). Nevertheless, as in the case of *Valonia*, each microfibril maintains its monocrystalline character during the initial phase of acetylation. As opposed to *Valonia* microfibrils, the contours of the unreacted cores of the partially acetylated tunicate microfibrils appear rounded.

The details in Figs 3 and 4 are schematized in Fig. 5 where the traces of a number of cellulose microfibrils sections before and after the first step of acetylation have been copied from a series of electron micrographs. With both, *Valonia* as well as tunicin, the onset of acetylation corresponds to a substantial decrease in the diameter of the crystalline cellulose microfibrils. With *Valonia*, this decrease seems to correspond more to losses of fragments. On the other hand, with tunicin, the decrease in diameter appears more like a smooth erosion mechanism.

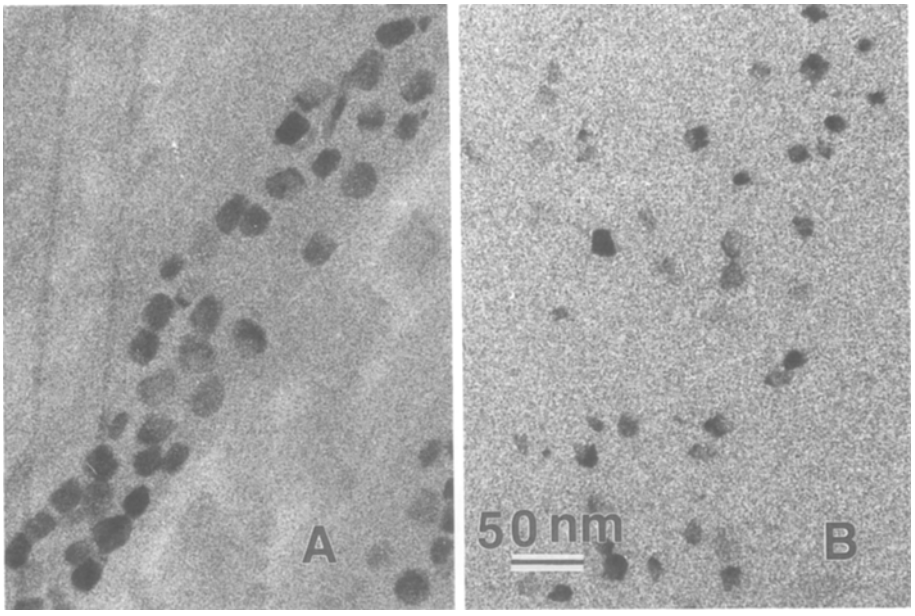

FIGURE 3. Electron micrographs of the cross sections of *Valonia* cell wall fragments before (3a) and after (3b) partial acetylation. The sections are made perpendicular to the microfibrillar directions. In the images, that are recorded in bright field mode in diffraction contrast transmission electron microscopy, the crystalline domains of cellulose are seen in black.

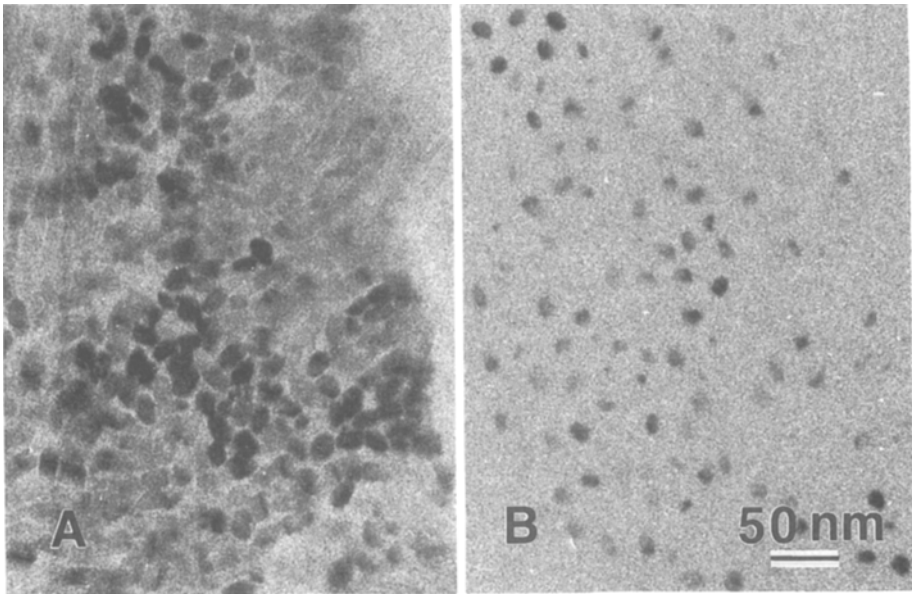

FIGURE 4. As in Fig 3 but with tunicate fragments from *Microcosmus fulcatus*.

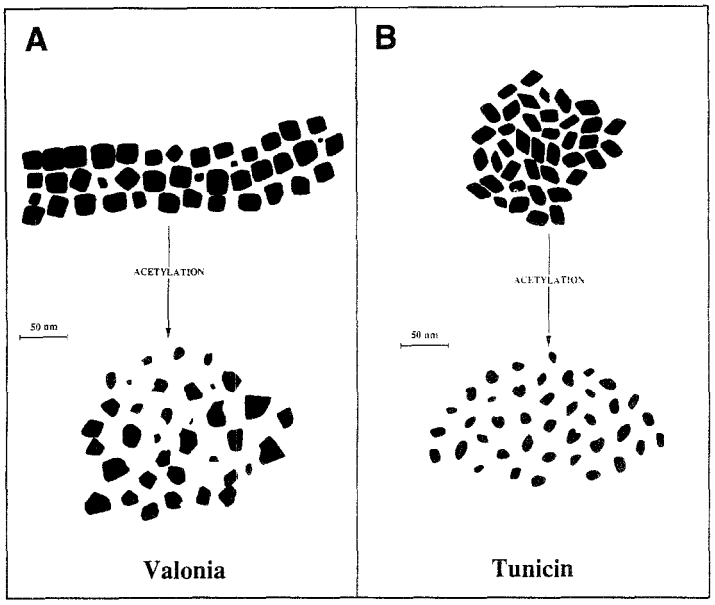

FIGURE 5. Schematic representation of the change in cross section of the cellulose crystals during partial acetylation. (a) Crystals from *Valonia* cellulose; (b) crystals from tunicin. The cross sectional shapes were directly traced from the electron micrographs taken during this study.

The ultrastructural modifications of cellulose crystals during acetylation can also be observed by the negative staining technique applied to individual cellulose microcrystals. This is illustrated in Figs 6a and b that correspond to a batch of microcrystals of tunicin before acetylation (Fig. 6a) and after the beginning of the reaction, when a DS of 0.17 has been reached (Fig. 6b). The initial tunicin crystals consist of long smooth elements having parallel edges, with longitudinal dimensions from one tenth of a micron to several microns. The crystals have variable lateral widths between 5 and 20 nm, most of them being, however, close to 20 nm. During acetylation, the tunicin crystals keep lengths similar to those of the original samples, but their diameter is drastically reduced. In addition, the crystals are no longer smooth but appear striated; their tip is frequently pointed, sometimes at one end, sometimes at both ends.

When the course of acetylation of cellulose crystals is followed by electron diffraction, the patterns display interesting features. This is illustrated in Fig. 7 where 7a corresponds to the initial sample, 7b to a sample of DS 2.41 and 7c to a sample of DS 2.81. The three patterns are of the powder type, i.e., they correspond to a distribution of crystals organized randomly. In Fig. 7a, the diagram consists of four inner rings calibrated at 0.6 (medium), 0.54 (medium), 0.44 (medium) and 0.40 nm (strong), together with a very sharp outer ring at 0.258 nm (medium). The three rings at 0.6, 0.54 and 0.4 nm correspond to the main equatorial planes indexed as $(1\,\bar{1}\,0)$, $(1\,1\,0)$ and $(0\,2\,0)$ if the monoclinic two-chain system defined by Sugiyama *et al.* (1991) for cellulose I_β is used. The reflection at 0.258 nm corresponds to the meridional planes, indexed as $(0\,0\,4)$ whereas the ring at 0.44 nm corresponds to the planes indexed as $(1\,0\,2)$ that are inclined with respect to the fiber axis. During acetylation, the intensity

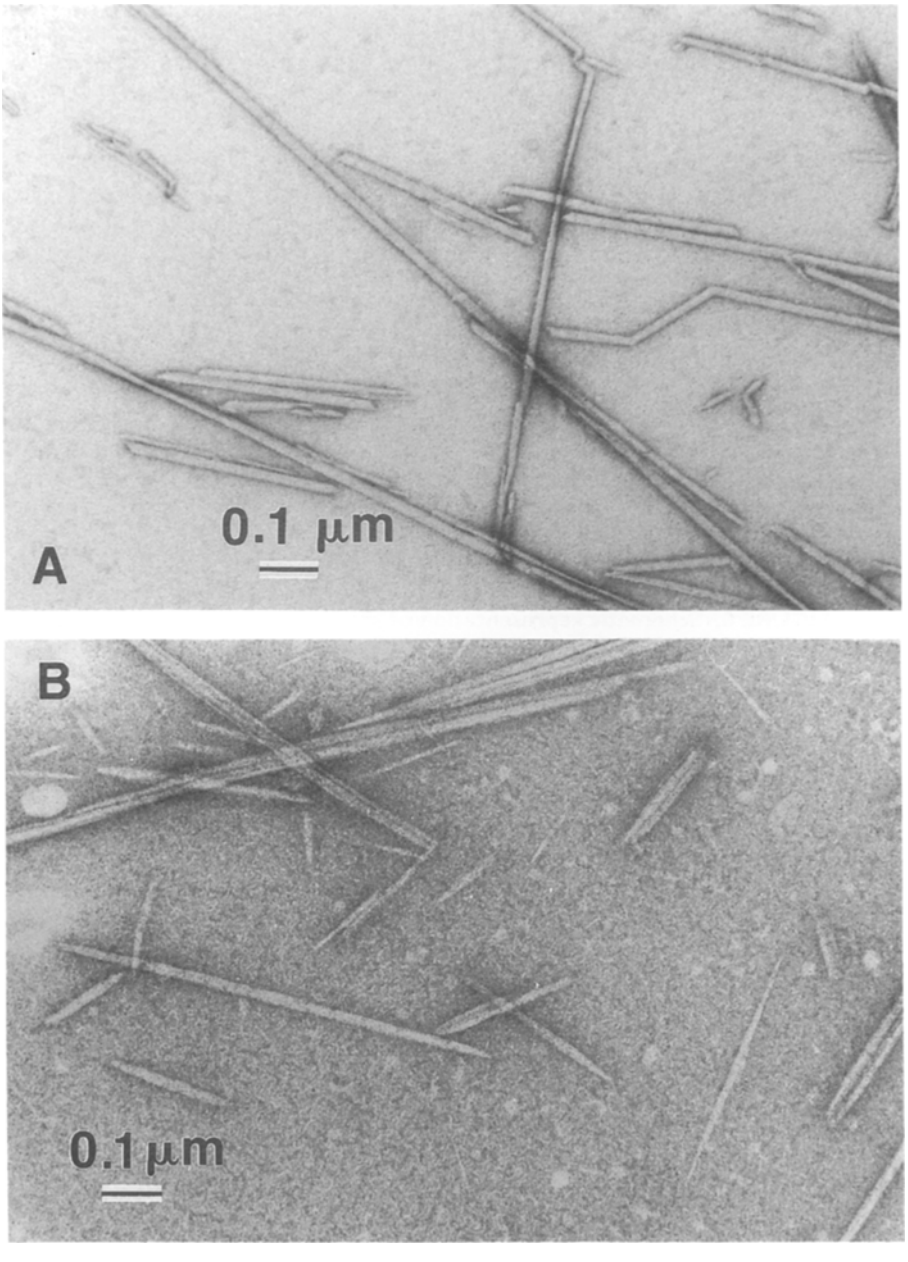

FIGURE 6. (a) Dispersion of microcrystals of tunicin before acetylation. (b) As in 6a but after partial acetylation to DS 0.17.

of the four inner diffraction rings decreases continuously to totally disappear when a DS of 2.8 is reached. On the other hand, the intensity of the meridional ring at 0.258 nm remains unaffected. Quite remarkably, in Fig. 7c, it is the only ring that is left, all the others having totally disappeared.

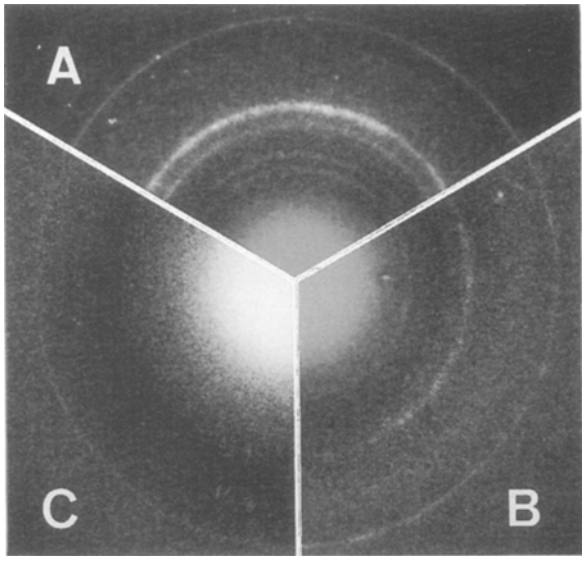

FIGURE 7. Electron diffraction diagrams of microcrystals of tunicin cellulose at different stages of acetylation and after removal of cellulose acetate by selective hydrolysis (Glegg *et al.*, 1968). (a) Initial; (b) sample of DS 2.41; (c) sample of DS 2.81.

The electron diffraction results are corroborated with X-ray data averaging much more specimens. Fig. 8 corresponds to a typical run where the conditions for an homogeneous acetylation were selected. After washing away the acetate, the remaining cellulose yields a series of X-ray diffractograms where (0 0 4) keeps its intensity whereas the three equatorial peaks corresponding to (1 $\bar{1}$ 0), (1 1 0) and (0 2 0) decrease steadily following the progress of acetylation. The interference (1 0 2) decreases also but to a lower extent. The case of fibrous acetylation appears to follow the same route (Fig. 9). In that case, however, the amount of acetate that is produced gives wide diffraction lines that cover many of the initial interferences of cellulose. Nevertheless, the diffraction peak corresponding to (0 0 4) stays constant up to a DS of 0.8 while the diffraction peaks corresponding to the equatorial planes of cellulose, especially the (0 2 0) at 0.40 nm, are drastically reduced.

Discussion

In this study, the course of cellulose acetylation and especially its onset have been followed on model substrates consisting of well dispersed cellulose crystals of large size and high perfection. Our electron microscopy data indicate that in both the homogeneous as well as the fibrous acetylation process, the cellulose crystals appear to be acetylated only on their surface. Thus the acetylation of cellulose does not lead to the crystalline swelling that is observed when cellulose is interacted with amines (Chanzy *et al.*, 1986). In the case of homogeneous acetylation, our observations are consistent with an acetylation mechanism consisting of a continuous stripping of the surface cellulose chains as they become acetylated. This will lead to a reduction in the diameter of the

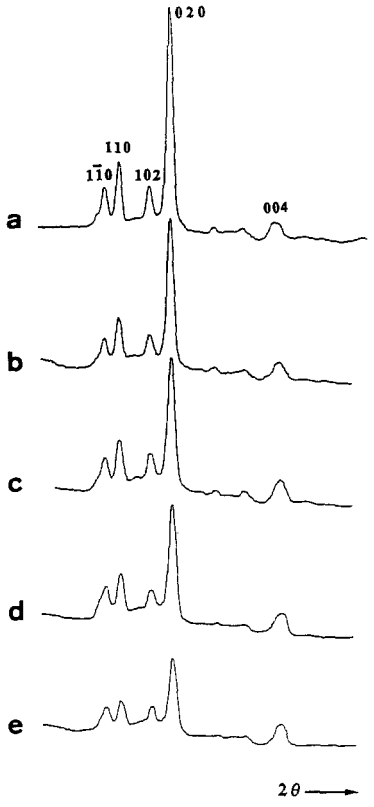

FIGURE 8. Microdensitometer tracings of the X-ray diffractograms of tunicin fragments at different stages of acetylation under homogeneous conditions. (a) Initial; (b) after 5 min of acetylation; (c) after 10 min of acetylation; (d) after 15 min of acetylation; (e) after 30 min of acetylation.

crystals while their longitudinal dimension stays either constant or is only slightly reduced.

In the case of fibrous acetylation, the cellulose acetate remains where it was produced and surrounds the unreacted core of the cellulose crystals. On the other hand, with homogeneous acetylation, as soon as a part of a cellulose chain located at the surface is sufficiently acetylated, it becomes soluble in the acetylating medium and is therefore lifted from the surface of the crystalline lattice. This phenomenon is schematically drawn in Fig. 10, which represents the onset of the acetylation of an isolated crystal of cellulose. In this model, the cellulose chains that are sufficiently acetylated to become soluble have left the crystal. As a consequence, the crystal becomes brittle as it is indented by a series of grooves corresponding to the missing cellulose chains. Three cellulose chains that are in the process of acetylation are also represented: their parts already rich in acetyl groups are sucked into the acetylating medium whereas their underivatized ends are still hooked into the crystalline lattice. In this scheme, it is likely that a surface cellulose chain that has started to be acetylated will easily be lifted completely from the crystal surface and thus its acetylation will be accelerated. This explains why the corresponding crystal is expected to shrink in

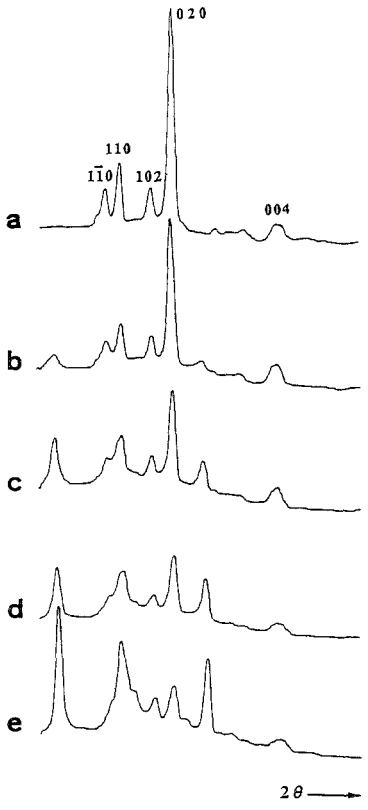

FIGURE 9. Microdensitometer tracings of the X-ray diffractograms of tunicin fragments at different stages of acetylation under heterogeneous conditions. (a) Initial; (b) after 5 min of acetylation (DS 0.2); (c) after 10 min of acetylation (DS 0.4); (d) after 15 min of acetylation (DS 0.8); (e) after 30 min of acetylation (DS 2.3).

diameter while its length will remain constant. In particular, the diagram in Fig. 10 explains also why the eroded crystals have frequently one or two pointed tips.

The course of the acetylation can also be followed by diffraction methods that have the advantage of giving average information on the crystalline state of a number of crystals. With electron diffraction techniques, the size of the sample is reduced and specific areas can be selected in preparations in which cellulose microcrystals are still seen despite a fairly high degree of substitution. With X-rays, the method is more representative of the total of a given sample as around 1 mm^3 of specimen is needed for the experiment. Both techniques reveal that during the initial stage of acetylation there is a continuous decrease in the intensity of the equatorial diffraction lines whereas that of the meridian lines is unaffected. For the diffraction lines that are neither on the meridian nor on the equator, their intensity decreases as a function of their azimuthal angle with respect to the fibre axis. These observations are schematically represented in Fig. 11 which corresponds to a fibre diffraction diagram of native cellulose. In this drawing, which is consistent with the data presented in Figs 5 and 6, the intensities of the strong equatorial spacings ($1\bar{1}0$), (110) and (020) decrease the most during

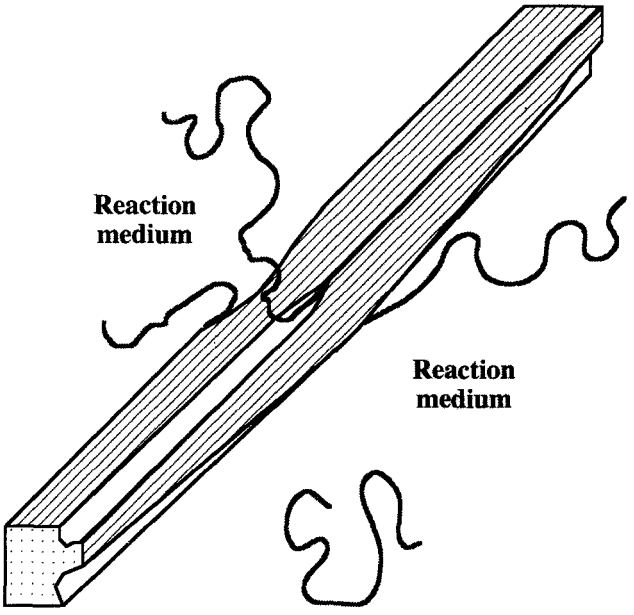

FIGURE 10. Schematic drawing describing the onset of the acetylation of a typical cellulose crystal. A chain that is sufficiently acetylated to become soluble has left the crystal. Three chains in the process of acetylation are partially lifted from the crystal. The crystal is indented by a series of grooves that correspond to the missing cellulose chains.

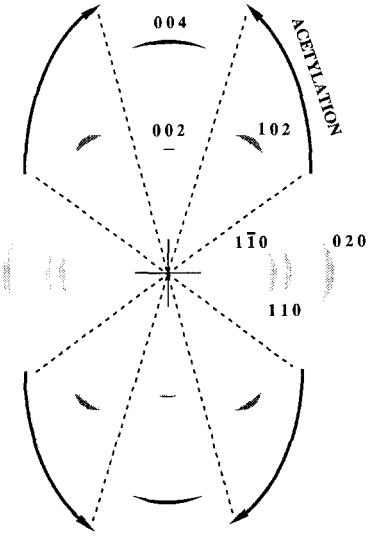

FIGURE 11. Schematic drawing showing the modification of the fibre diffraction pattern of cellulose during acetylation. The diagram shows three sectors, with the azimuthal arrows pointing in the direction of increasing retained order as acetylation progresses.

acetylation. The intensity of the medium reflection (102), diffracting at 0.438 nm, is also reduced but to a lesser extent. Finally, the meridional reflections (002) and (004) are unaffected, at least during the first phase of acetylation. An illustration of this phenomenon is presented in Fig. 7c where some areas in the sample show only a sharp (004) diffraction line whereas all the remaining diffraction has disappeared. In such a case, only the longitudinal order of the crystals is preserved while all lateral perfection has disappeared, probably due to rotational disorder while the crystallographic translation is kept. Such an observation is consistent with our model of acetylation described in Fig. 10 where the crystals break down laterally but not longitudinally.

A close survey of the evolution of the X-ray and electron diffractograms of the cellulose specimens during acetylation reveals interesting behaviour since the decrease in the intensities of the equatorial diffraction lines is not accompanied by a significant line broadening. On the other hand, the meridional diffraction lines keep their intensities and sharpness. The disappearance of equatorial diffractions without line broadening is consistent with an 'all or nothing' acetylation process in which the rate for a given crystal would autoaccelerate with the onset of acetylation. Indeed, our diffraction observations seem to indicate that as soon as a crystal starts to be acetylated, it derivatizes completely. Therefore, there will never be any build up of intermediate crystals of reduced diameters giving a line broadening effect on the equatorial spacings of their diffraction. The occurrence of a substantial amount of disordered crystals diffracting as in Fig. 7c and responsible for the persistence of a fairly intense and narrow meridional reflection is however quite unexpected. Obviously, these disordered crystals have kept their coherence along the crystal length with little or no coherence laterally, since all equatorial diffraction information is lost. During acetylation, the percentage of disordered crystals seems to be increasing since the ratio of the intensity of the meridional (004) versus that of the equatorial (020) increases steadily. It is tempting to propose a mechanism whereby the occurrence of a disordered crystal would correspond to an intermediate step reached by the cellulose crystal during its acetylation and before its total dissolution. The reason for the build up of such an intermediate step is at present unclear. Also, the exact morphology and description of such disordered crystals yielding only one sharp meridional diffraction spot remains to be clarified.

The occurrence of a population of similar disordered cellulose crystals is not new as it was observed also during the enzymatic digestion of crystalline cellulose. In fact the electron diffractograms that are observed here are quite similar to those resulting from the interaction of cellobiohydrolase 1 (CBH1) and *Valonia* cellulose (Chanzy and Henrissat, 1983, Henrissat and Chanzy, 1986). This similarity can be explained by the fact that both the above acetylation mechanism as well as the enzymatic attack are occurring at the surface of the cellulose crystals and progressing towards their center. Despite this similarity, the molecular description of cellulose crystals giving only a sharp diffraction line remains to be made.

The acetylation mechanism presented in this study is consistent with the acetylation models presented by Sisson (1938) or Glegg *et al.* (1968). Yet, these authors have deduced their model from X-ray diffraction measurements only. They described the crystal erosion as occurring not only along the diameter of the crystals but also along their length. Our results go one step further as they present not only diffraction patterns but also images of the cellulose crystals during their acetylation. Our observa-

tions allow therefore a model of acetylation to be proposed such as that shown in Fig. 10, which is more exact. This model applies however to quasi-perfect cellulose crystals. It remains to be seen whether this situation can be transposed to industrial systems where the acetylation is applied to cotton linters or cellulose from wood pulp.

ACKNOWLEDGEMENTS

The authors acknowledge Dr E. Fleury from Rhône-Poulenc for valuable suggestions during this work. One of us (J.- F. S.) was a recipient of a Rhône-Poulenc fellowship. R. H. Marchessault provided stimulating exchanges during revision of the manuscript.

REFERENCES

Bachhuber, K. and Frösch, D. (1983) Melamine resins, a new class of water-soluble embedding media for electron microscopy. *J. Microsc.* **130**, 1–9.

Buras, E. M., Jr., Hobart, S. R., Hamalainen, C. and Cooper, A. S., Jr. (1957) A preliminary report on fully acetylated cotton. *Textile Res. J.* **27**, 214–222.

Chanzy, H. and Henrissat, B. (1983) Electron microscopy study of the enzymatic hydrolysis of *Valonia* cellulose. *Carbohydr. Polym.* **3**, 161–173.

Chanzy, H., Henrissat, B., Vuong, R. and Revol, J.-F. (1986) Structural changes of cellulose crystals during the reversible transformation cellulose I→III in *Valonia*. *Holzforshung* **40**(Suppl.), 25–30.

Chanzy, H. (1990) Aspects of cellulose structure. In Cellulose Sources and Exploitation. (J. F. Kennedy, G. O. Phillips and P. A. Williams, eds) New York: Ellis Horwood pp. 3–12.

Conrad, C. M. and Creely, J. J. (1962) Thermal X-ray diffraction study of highly acetylated cotton cellulose. *J. Polym. Sci.* **58**, 781–790.

Gardner, K. H. and Blackwell, J. (1974) The structure of native cellulose. *Biopolymers* **13**, 1975–2001.

Glegg, R. E., Ingerick, D., Parmerter, R. R., Salzer, J. S. T. and Warburton, R. S. (1968) Acetylation of cellulose I and II studied by limiting viscosity and X-ray diffraction. *J. Polym. Sci., Part A2* **6**, 745–773.

Henrissat, B. and Chanzy, H. (1986) Enzymatic breakdown of cellulose crystals. In *Cellulose: Structure, Modification and Hydrolysis*. (R. A. Young and R. M. Rowell eds) New York: Wiley Interscience, pp 337–347.

Hess, K. and Schultze, G. (1927) Über die präparative Abscheidung von Cellulosekrystallen aus Bastfasern. *Justus Liebigs Ann. Chem.* **456**, 55–68.

Hess, K. and Trogus, C. (1931) Zur Kenntnis der Reaktionsweise der Cellulose. *Z. Physik. Chem.* **B 15**, 157–222.

Hurtubise, F. G. (1962) The analytical and structural aspects of the infrared spectroscopy of cellulose acetate. *Tappi J.* **45**, 460–465.

Kanamaru, K. (1934) Über das Lichtbrechungsvermögen der Cellulose und ihrer Derivate. IV. Die Brechungsindices von Nitrocellulose und Acetylcellulose. *Helv. Chim. Acta* **17**, 1436–1440.

Kuga, S. and Brown, R. M., Jr. (1987a) Practical aspects of lattice imaging of cellulose. *J. Electron Microsc. Technique* **6**, 349–356.

Kuga, S. and Brown, R. M., Jr. (1987b) Lattice imaging of ramie cellulose. *Polymer Commun* **28**, 311–314.

Malm, C. J., Tanghe, L. J. and Laird, B. C. (1946) Preparation of cellulose acetate. Action of sulfuric acid. *Ind. Eng. Chem.* **38**, 77–82.

Revol, J.-F. (1982) On the cross-sectional shape of cellulose crystallites in *Valonia ventricosa*. *Carbohydr. Polym.* **2**, 123–134.

Revol, J.-F. and Goring, D. A. I. (1983) Directionality of the fibre *c* axis of cellulose crystallites in microfibrils of *Valonia ventricosa*. *Polymer* **24**, 1547–1550.

Revol, J.-F. (1985) Change of the *d* spacing in cellulose crystals during lattice imaging. *J. Mater. Sci. Lett.* **4**, 1347–1349.

Revol, J.-F., Bradford, H., Giasson, J., Marchessault, R. H. and Gray, D. G. (1992) Helicoidal self-ordering of cellulose microfibrils in aqueous suspension. *Int. J. Biol. Macromol.* **14**, 170–172.

Serad, G. A. (1985) in Encyclopedia of Polymer Science and Engineering, Volume 3 (H. F. Mark, N. M. Bikales, C. G. Overberger and G. Menges eds) New York: Wiley Interscience, pp. 200–226.

Sisson, W. A. (1938) X-ray diffraction behavior of cellulose derivatives. *Ind. Eng. Chem.* **30**, 530–537.

Sprague, B. S., Riley, J. L. and Noether, H. D. (1958) Factors influencing the crystal structure of cellulose triacetate. *Textile Res. J.* **28**, 275–287.

Staudinger, H., In den Birken, K.-H. and Staudinger, M. (1953) Über den micellaren oder makromolekularen Bau der Cellulosen. *Makromol. Chem.* **9**, 148–187.

Sugiyama, J., Harada, H., Fujiyoshi, Y. and Uyeda, N. (1985a) Observations of cellulose microfibrils in *Valonia macrophysa* by high resolution electron microscopy. *Mokuzai Gakkaishi* **31**, 61–67.

Sugiyama, J., Harada, H., Fujiyoshi, Y. and Uyeda, N. (1985b) Lattice imaging from ultrathin sections of cellulose microfibrils in the cell wall of *Valonia macrophysa* Kütz. *Planta* **166**, 161–168.

Sugiyama, J., Vuong, R. and Chanzy, H. (1991) Electron diffraction study on the two crystalline phases occurring in native cellulose from an algal cell wall. *Macromolecules* **24**, 4168–4175.

Tanghe, L. J., Genung, L. B. and Mench, J. W. (1963) Cellulose acetate. Acetylation of cellulose. In Methods in Carbohydrate Chemistry, Volume III, Cellulose (R. L. Whistler, J. W. Green, J. N. BeMiller and M. L. Wolfrom eds.) New York: Academic Press, pp. 193–198.

Van Daele, Y., Revol, J.-F., Gaill, F. and Goffinet, G. (1992) Characterization and supramolecular architecture of the cellulose-protein fibrils in the tunic of the sea peach (*Halocynthia papillosa*, Ascidiacea, Urochordata). *Biol. Cell* **76**, 87–96.